



Symmetry Breaking in Dynamical Encounters in the Disks of Active Galactic Nuclei

Yi-Han Wang¹ , Barry McKernan^{2,3} , Saavik Ford^{2,3}, Rosalba Perna^{1,3} , Nathan W. C. Leigh^{1,4,5} , and Mordecai-Mark Mac Low⁵

¹ Department of Physics and Astronomy, Stony Brook University, Stony Brook, NY 11794-3800, USA; yihan.wang.1@stonybrook.edu

² Department of Science, BMCC, City University of New York, New York, NY 10007, USA

³ Center for Computational Astrophysics, Flatiron Institute, New York, NY 10010, USA

⁴ Departamento de Astronomía, Facultad Ciencias Físicas y Matemáticas, Universidad de Concepción, Av. Esteban Iturra s/n Barrio Universitario, Casilla 160-C, Concepción, Chile

⁵ Department of Astrophysics, American Museum of Natural History, New York, NY 10024, USA

Received 2021 October 7; revised 2021 November 24; accepted 2021 November 26; published 2021 December 16

Abstract

The disks of active galactic nuclei (AGNs) may be important sites of binary black hole (BBH) mergers. Here we show via numerical experiments with the high-accuracy, high-precision code `SpaceHub` that broken symmetry in dynamical encounters in AGN disks can lead to asymmetry between prograde and retrograde BBH mergers. The direction of the hardening asymmetry depends on the initial binary semimajor axis. Under the assumption that the spin of the BHs becomes aligned with the angular momentum of the disk on a short timescale compared with the encounter timescale, an asymmetric distribution of mass-weighted projected spin χ_{eff} is predicted in LIGO–Virgo detections of BBH mergers from AGN disks. In particular, this model predicts that positive χ_{eff} BBH mergers are most likely for encounters with massive tertiaries in migration traps at radial distances $\gtrsim 500\text{--}600$ gravitational radii.

Unified Astronomy Thesaurus concepts: Active galactic nuclei (16); Black hole physics (159); Stellar dynamics (1596); Stellar mass black holes (1611); A supergiant stars (8); Supermassive black holes (1663); Dynamical friction (422); Gravitational waves (678)

1. Introduction

The disks of active galactic nuclei (AGNs) disks may be important sites for stellar-mass binary black hole (BBH) mergers (McKernan et al. 2012; Bartos et al. 2017; Stone et al. 2017; Leigh et al. 2018; Samsing et al. 2020), but the detailed processes that lead to a BBH merger in an AGN disk are not yet well constrained (e.g., McKernan et al. 2018; Gröbner et al. 2020). We expect that binary formation in AGN disks is extremely efficient (Secunda et al. 2020; Tagawa et al. 2020a) and that initial binary hardening will occur due to gas drag (e.g., Baruteau et al. 2011, but see also Li et al. 2021; Tiede et al. 2020). However, we expect gas drag will eventually become inefficient (e.g., Leigh et al. 2014), leading to binaries that stall at semimajor axes too large for a gravitational wave-driven merger to occur in less than the AGN disk lifetime. Thus, dynamical encounters could play a critical role in hardening (or disrupting) binaries in the AGN channel (e.g., Leigh et al. 2018; Secunda et al. 2020; Samsing et al. 2020; Tagawa et al. 2020b). The imprint of dynamical processes particular to AGN disks could appear in the gravitational wave signal of such BBH mergers.

Within the LIGO–Virgo detected population of BBH mergers, an intriguing anticorrelation may have been detected between the mass ratio of binaries with masses M_1 and M_2 and the mass-weighted projection of spin onto binary orbital angular momentum χ_{eff} (Callister et al. 2021). Most dynamical channels for BBH mergers are rotationally symmetric and therefore predict a symmetric distribution of χ_{eff} around

$\chi_{\text{eff}} = 0$ (e.g., Rodriguez et al. 2018; Liu & Lai 2017). However, McKernan et al. (2021) point out that there are several natural sources of symmetry breaking in the AGN channel for BBH mergers. Figure 1 shows BBHs in an AGN disk with binary angular momenta oriented (anti-)parallel to the disk angular momentum and hence (retrograde) prograde compared to the disk-gas angular momentum. Hereafter, we denote prograde and retrograde binaries as (+) or (−), respectively, and prograde or retrograde tertiaries as + or −.

There are several forms of symmetry breaking relevant to the encounters described below. (1) A binary more massive than tertiary objects in an AGN disk will migrate faster than any tertiaries and therefore will frequently encounter less massive, slower migrating, tertiary objects on interior orbits while migrating, though equal-mass encounters due to recently captured or merged objects are also possible. (2) A stalled binary at a migration trap will *mostly* experience tertiary encounters from exterior orbits since migration traps tend to occur in the inner disk (Bellovary et al. 2016) and migration is usually directed radially inward. (3) BHs with an initially random spin alignment only need to accrete 1%–10% of their own mass from the gas disk to bring their spins into alignment with the angular momentum of the disk (Bogdanović et al. 2007). The timescale for this accretion process is usually shorter than the timescale for the BHs to migrate to the trap. Thus, we can assume that the spins of the disk BHs are aligned with the angular momentum of the disk before scattering (hence either aligned or antialigned with the orbital angular momentum of the binaries).

Points (1) and (2) suggest we should expect a bias in the directionality of dynamical encounters in AGN disks, while point (3) suggests that BH spins should be biased *toward* alignment with the disk. A combination of these factors implies we should expect asymmetry in the expected χ_{eff} distribution from this channel.



Original content from this work may be used under the terms of the [Creative Commons Attribution 4.0 licence](https://creativecommons.org/licenses/by/4.0/). Any further distribution of this work must maintain attribution to the author(s) and the title of the work, journal citation and DOI.

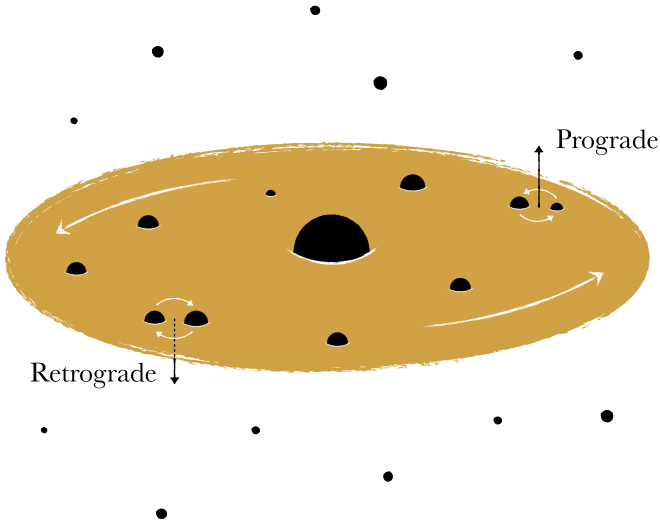


Figure 1. Prograde vs. retrograde binaries: single BHs in an AGN disk that are orbiting the SMBH with their angular momentum aligned to the disk angular momentum L_d will form binaries whose center of mass will continue to orbit with the disk gas. However, the orbital angular momentum of the binary around its own center of mass may be either prograde (aligned with L_d) or retrograde (antialigned with L_d). We use the terms “prograde” (+) and “retrograde” (−) binary, respectively, for these two arrangements. (Figure credit: T. Callister 2021, personal communication).

McKernan et al. (2021) argued that: (1) the hard–soft boundary for (+) and (−) binaries should be different for tertiary encounters from a preferred direction (i.e., different hard–soft boundaries for (+),+ and (−),+ and (2) more massive (−) binaries are more probable survivors of + tertiary encounters. In this Letter we test and quantify these hypotheses via numerical scattering experiments.

2. Numerical Methods

The scattering experiments are performed using our high-precision, few-body code `SpaceHub` (Wang et al. 2021), which employs several novel algorithms shown to outperform other numerical methods in the literature for both accuracy and precision. For the scattering experiments performed for this work, since the mass ratio between the stellar-mass black hole (BH) and the supermassive black hole (SMBH) is very small, and the scattering may involve extreme eccentricities, we use the `AR-chain+` method in `SpaceHub`, which can deal with systems with extreme eccentricity and low-mass ratios accurately and precisely. Post-Newtonian (PN) general relativity terms are included as pairwise interactions. We include the first order (precession), second order (correction to precession), and 2.5th order terms in the acceleration (gravitational radiation). No significant differences are found in our simulation results after we include these PN terms.

We set up coplanar scattering experiments between equal-mass prograde (+) or retrograde (−) BBHs and prograde tertiaries on outer orbits. Each BH in the binary has a mass $30 M_\odot$, and a single + tertiary BH with mass 10, 30, or $60 M_\odot$. The initial (i.e., pre-scattering) eccentricity of the BBH is set to be zero since the gas in the AGN disk is expected to circularize the dynamically formed BBH on a very short timescale compared to the dynamical time of the encounters (Theuns et al. 1996). The relative velocity v_∞ between the single BH

and the BBH is assumed to be 50 km s^{-1} , the order of magnitude expected for encounters in an AGN disk. A $10^8 M_\odot$ central SMBH particle is included in the simulations. We explored different distances between the SMBH and the BBH of 10, 5, 3, and $2 R_{\text{TDE}}$, where

$$R_{\text{TDE}} = \left(\frac{M_{\text{SMBH}}}{M_{\text{BBH}}} \right)^{1/3} a_{\text{BBH}} \quad (1)$$

is the tidal disruption radius of the BBH, which can be parameterized as

$$R_{\text{TDE}} \sim 120 r_g \left(\frac{M_{\text{SMBH}}}{10^8 M_\odot} \right)^{1/3} \left(\frac{M_{\text{BBH}}}{60 M_\odot} \right)^{-1/3} \left(\frac{a_{\text{BBH}}}{1 \text{ au}} \right) \quad (2)$$

for $r_g = GM_{\text{SMBH}}/c^2 \sim 1 \text{ au} (M_{\text{SMBH}}/10^8 M_\odot)$. Thus $2\text{--}10 R_{\text{TDE}}$ spans $\sim 200\text{--}1000 r_g$ in a disk around an $M_{\text{SMBH}} \sim 10^8 M_\odot$ SMBH. This includes regions where a migration trap may exist in the disk (Bellovary et al. 2016; Yang et al. 2019; Samsing et al. 2020; Secunda et al. 2020; Tagawa et al. 2020a, but see also Dittmann & Miller 2020). The range of distances between the SMBH and the binary is chosen so that it straddles the two limits of the binary being tidally disrupted by the SMBH due to the Hills (1988) mechanism and the SMBH not having any significant influence on the scattering event. The latter limit can be seen by comparison with reference-scattering experiments which we further performed without the SMBH. For each set of parameters, one million scattering experiments are performed to obtain statistically significant results.

3. Results from Scattering Experiments

The results of our scattering experiments are displayed as phase-space maps in the plane of impact parameter b and initial BBH phase ϕ_0 in Figures 2, 3, and 4 for three values of the mass of the tertiary BH: 30, 10, and $60 M_\odot$, respectively. The value $\phi_0 = 0$ corresponds to the configuration where the two BHs in the binary are aligned with the tertiary at infinity. Note that only the range $(0, \pi)$ is shown since the phase space is symmetric around π for equal-mass BHs.

In Figure 2, there is a clear visual difference between prograde (+) binaries on the left-hand side (LHS) and retrograde (−) binaries on the right-hand side (RHS). Far from the SMBH or absent from its influence, there is a larger region of binary hardening parameter space (in yellow) among + tertiary encounters with (+) binaries (LHS), compared with the same region for (−) binaries (RHS). The difference corresponds to a roughly 3:1 hardening ratio across phase space for encounters neglecting the SMBH (top row). The asymmetry occurs because + tertiaries scatter from (+) and (−) binaries with different relative velocities. This leads to a different hard–soft boundary for (+) and (−) binaries relative to + encounters. On average, a + tertiary encounter with a (−) binary contains more relative kinetic energy at encounter due to the larger velocity differential. In particular, close + encounters (at relatively small impact parameters) are far more likely to soften (−) binaries than (+) binaries (e.g., Leigh et al. 2018).

We see a difference in outcomes when we drop the mass of the + tertiary encounter to $10 M_\odot$ in Figure 3. In this case, the hardening fraction of parameter space (again in yellow) is similar for both (+) and (−) binaries if the BBH is far away

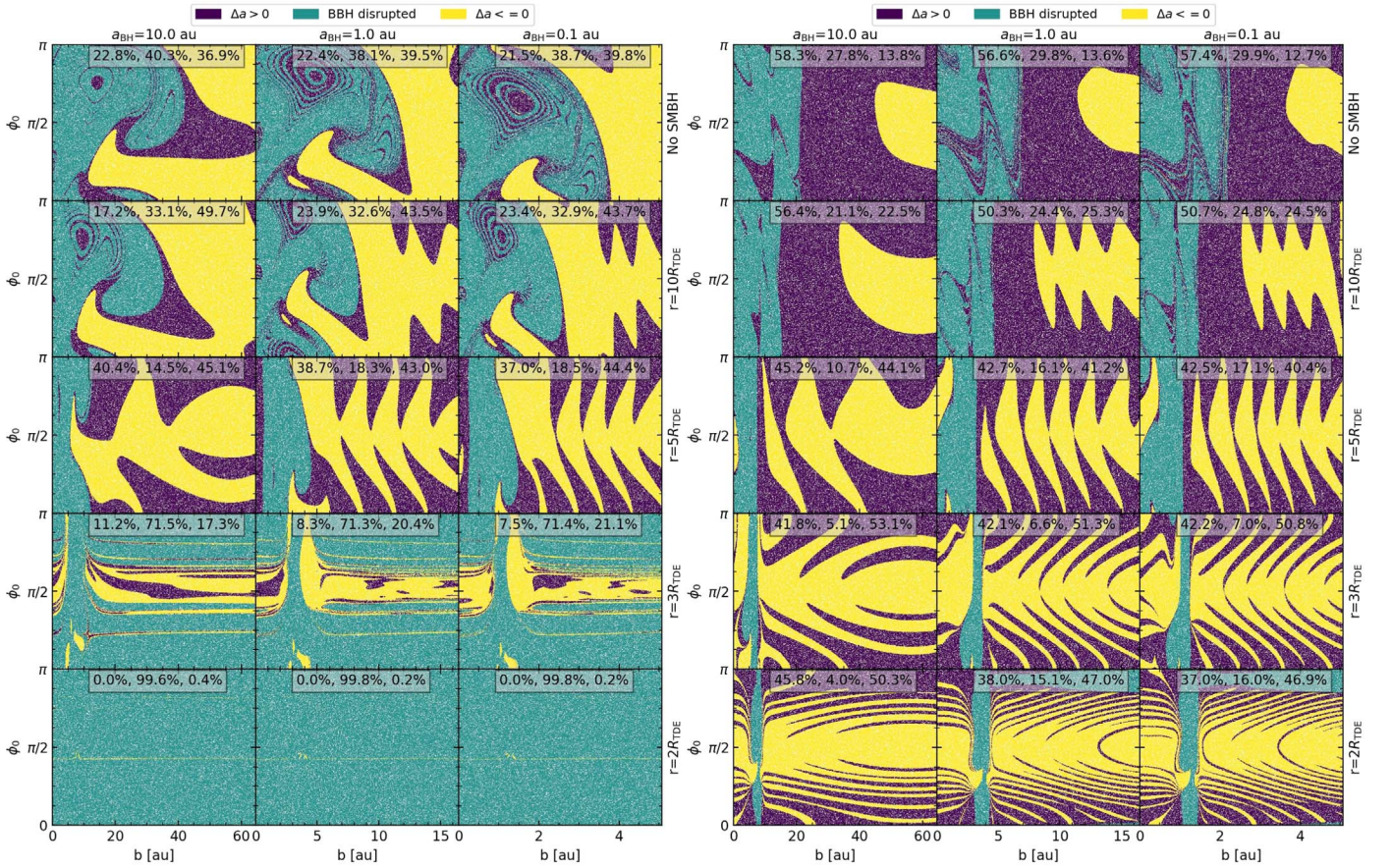


Figure 2. Outcome of the scatterings between a (+) BBH (LHS) or a (-) BBH (RHS) and a + tertiary BH as a function of the initial phase of the BBH ϕ_0 , where $\phi_0 = 0$ corresponds to the configuration with the two BHs aligned with the tertiary at infinity and impact parameter b of the tertiary BH. The masses of the BHs in the (+, -) binary are both $30 M_\odot$, while the mass of the + tertiary is also $30 M_\odot$. The left panels show the results for a (+), + encounter, while the right panels show the results for a (-), + encounter. The radius of the encounter from the central SMBH is shown on the right. The percentage of encounters that soften, disrupt, or harden the BBH are given at the top of each subplot.

from the SMBH. Since the energy and angular momentum carried by the tertiary is smaller than for the case with a $30 M_\odot$ tertiary, the encounters show less asymmetry between (+) and (-) binaries. Finally, encounters with more massive $60 M_\odot$ + tertiaries lead to a higher rate of binary softening or ionization among both the (+) and (-) binaries, but the hardening ratio (yellow) across all of the parameter space remains similar at around $\sim 3:1$ for the cases without an SMBH.

An intriguing feature of Figures 2, 3, and 4 is the somewhat periodic behavior displayed by the phase-space regions with softening and hardening scattering outcomes (respectively, the purple and yellow regions in those figures) in the simulations when an SMBH is present. We interpret these features as the coupled result of two effects: (1) the tidal force from the SMBH causes a time-dependent distortion of the circular orbit of the binary, with a pattern that is periodic with respect to the orbital period of the binary, and (2) as the impact parameter of the scatterer varies (and so does the time to reach the point of closest approach), the scatterer approaches the binary at its closest point at different orbital phases. The combination of (1) and (2) results in periodic closest approaches of the tertiary to the binary in a certain tidally deformed shape, which then influences the degree by which it is hardened or softened by scattering.

The trends discussed above are further modified if the scattering happens near the SMBH. At large disk radii (second row from top), the trends are similar to the case of no SMBH: (+) binaries are more likely disrupted in the encounters, whereas (-) binaries are more likely softened. At small impact parameters, the encounter is *always* ionizing or softening for (-) binaries, whereas for (+) binaries, small impact parameters can still lead to binary hardening. However, we can see that, as the distance of the BBH from the SMBH gets smaller (i.e., moving toward the lower panels of Figures 2–4), the tidal force from the SMBH starts to dominate the BBH system over the scatterings from the + tertiary, leading to more extended softening areas in these subplots (due to tidal softening by the SMBH). As the distance from the SMBH approaches $2 R_{\text{TDE}}$, the BBH fate is dominated by tidal disruption, as expected.

If we define A_{hard} as the area of phase space in which a binary is hardened, then we can compare $A_{\text{hard},(+),+}$, the fraction of (+) BBHs that are hardened by a + tertiary encounter, to $A_{\text{hard},(-),+}$, the fraction of (-) BBHs that are hardened by a + tertiary encounter. This ratio is shown in the upper panel of Figure 5. The bottom panel of the same figure shows the same area ratios, but including only those postscattered binaries whose merger times due to gravitational radiation (as a function of semimajor axis and eccentricity) are smaller than a Hubble time. The middle panel shows the fraction of scatterings that lead to binaries in this GW regime. It

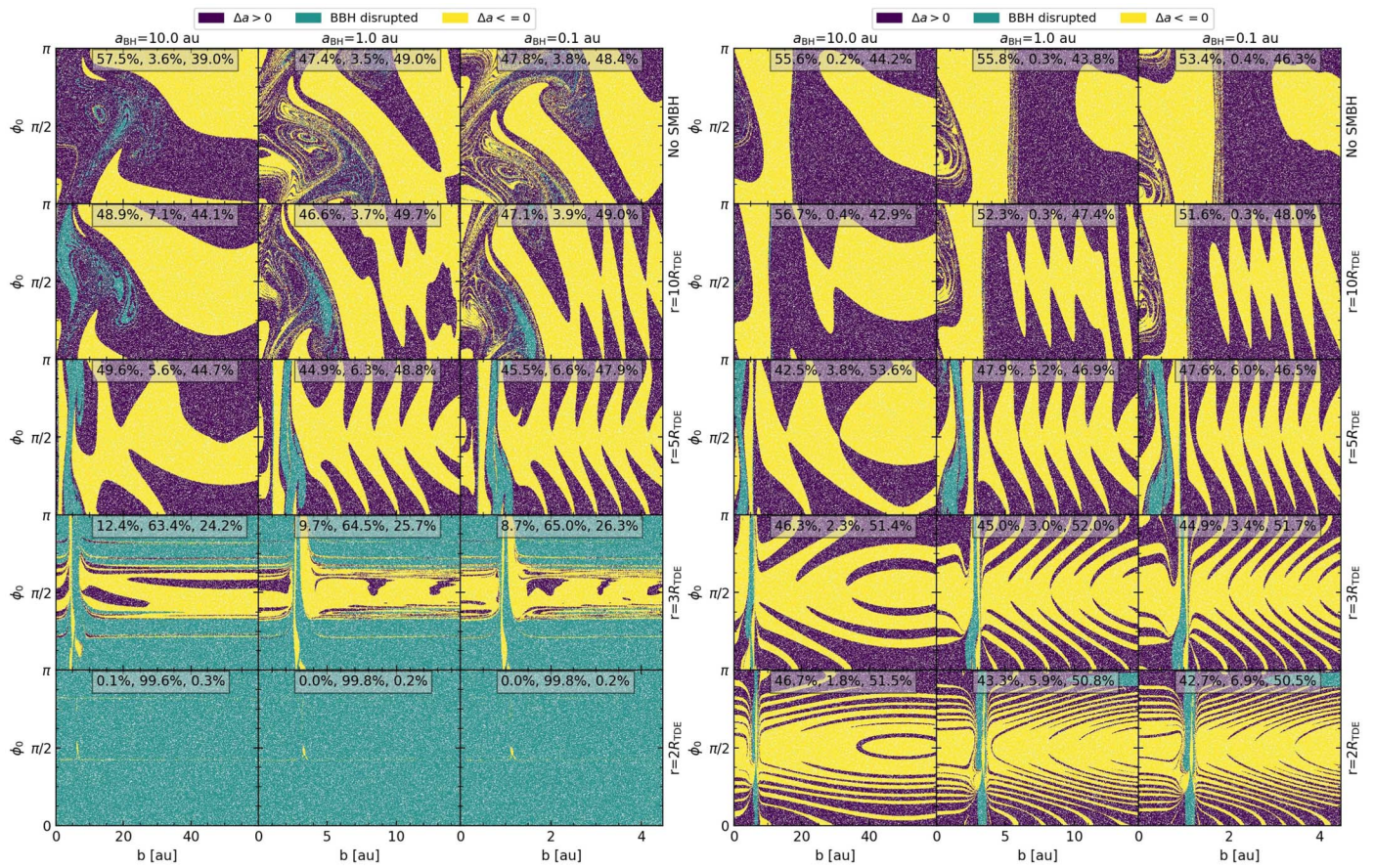


Figure 3. Same as in Figure 2 but for a lower mass + tertiary with mass $10 M_{\odot}$.

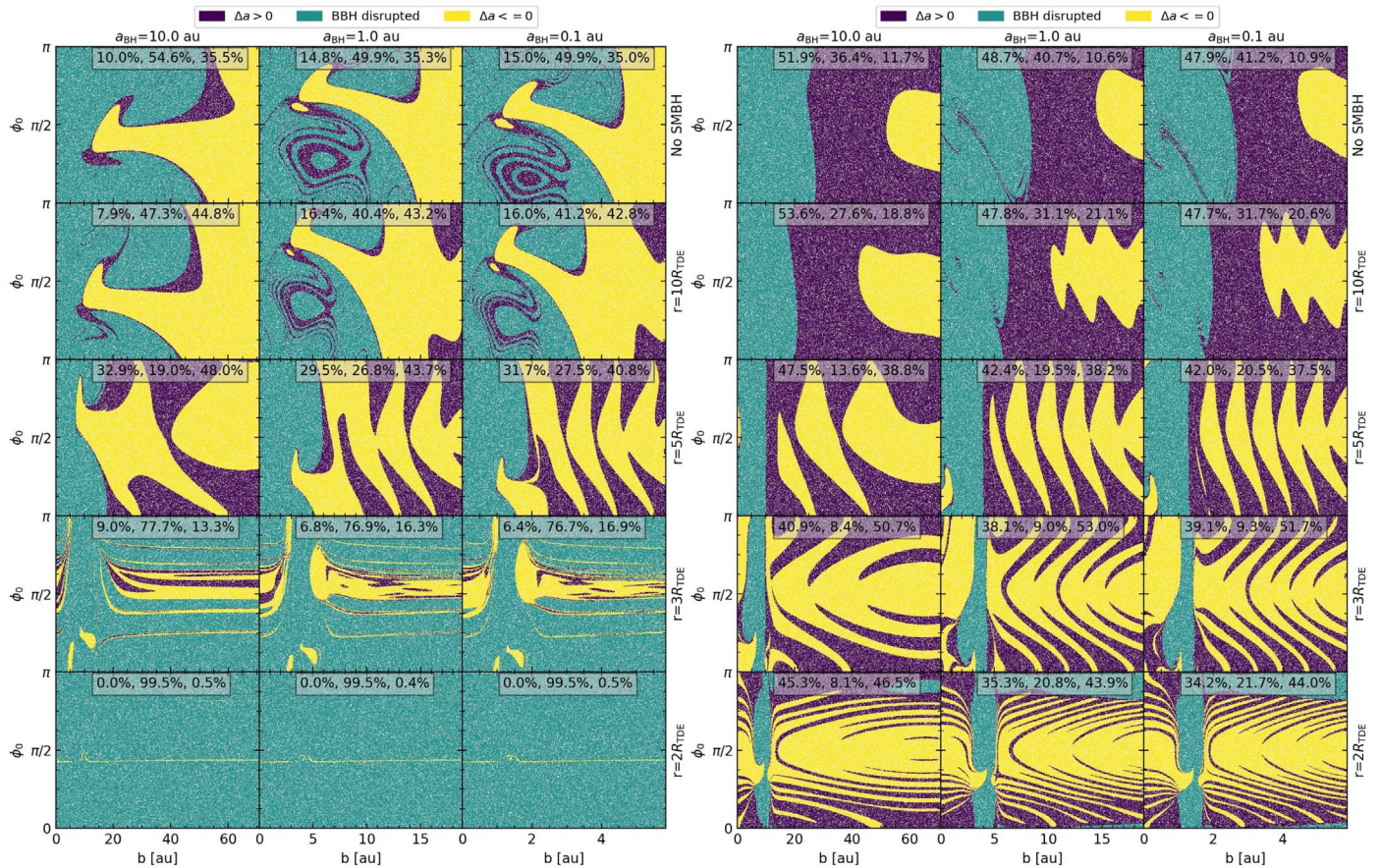


Figure 4. Same as in Figure 3 but for a higher-mass tertiary with mass $60 M_{\odot}$.

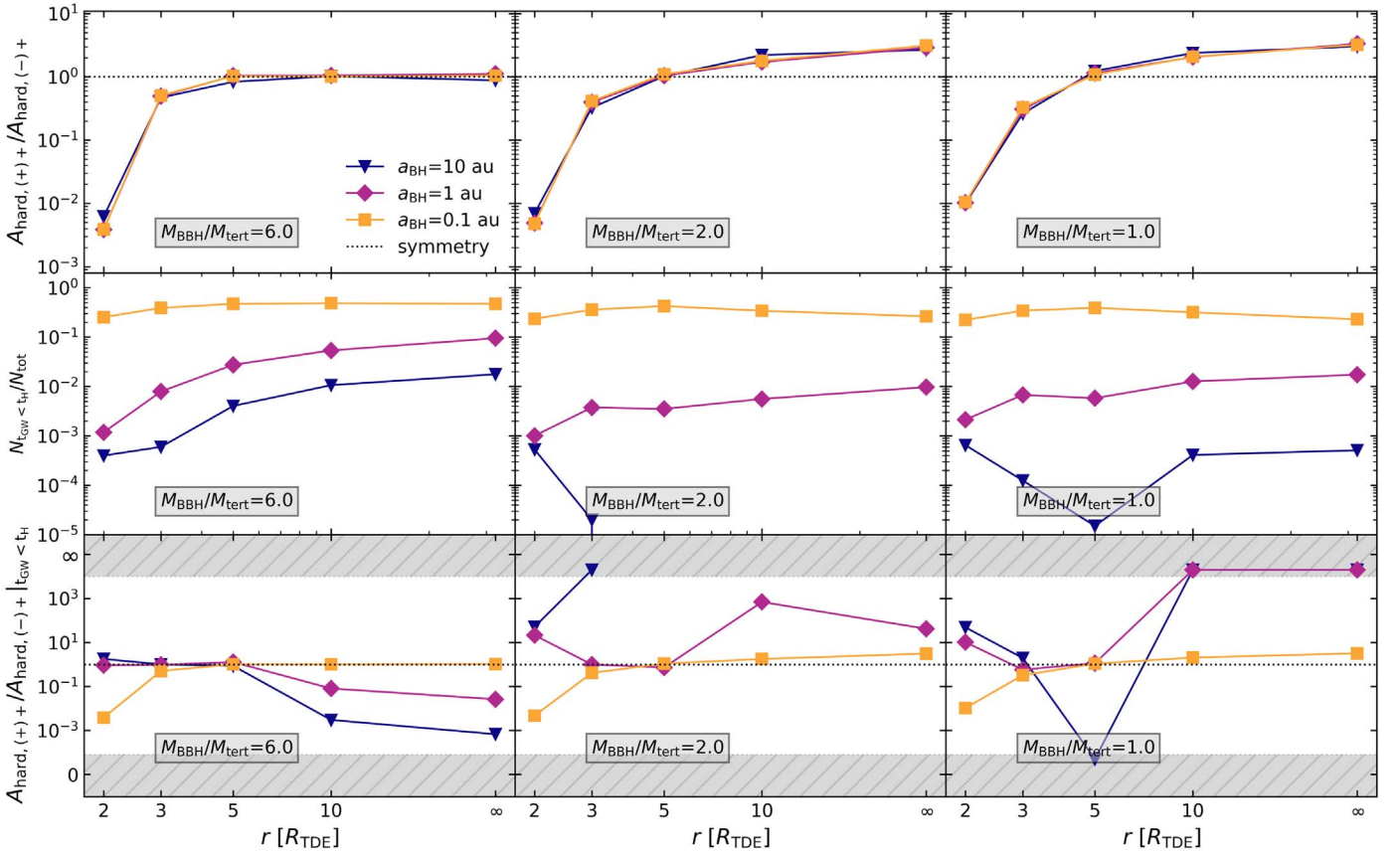


Figure 5. Ratio between the phase-space areas of hardened prograde and retrograde binaries for the full sample of hardened binaries (top row), and for the subset with merger times smaller than the Hubble time (bottom row). The middle row shows the fraction of all binaries satisfying the Hubble time criterion. The three columns show the variation with tertiary mass ($M = 10 M_{\odot}$ in the left panels, $M = 30 M_{\odot}$ in the middle panels, and $M = 60 M_{\odot}$ in the right panels). Some points for $a_{\text{BH}} = 10$ au in the bottom middle and right panels are missing as the corresponding area ratios are not well defined due to both areas being infinitesimally small, while the points at ∞ on the y-axis (within the shaded area) represent cases where only the area term in the denominator, $(+)-$, is infinitesimally small. Note that the x-axis is logarithmic with a base of 2, but has a discontinuity at the arrow; the points at ∞ on the x-axis refer to the simulations with no SMBH. Also note that the simulations with $a_{\text{BH}} = 10$ au and 1 au at $r \leq 3R_{\text{TDE}}$ have only a very small fraction ($<1\%$) of BBHs which are in the GW regime (especially for $(+)$ binaries). The error on the ratio for these binaries is $\sim 10^3$, which does not yield enough statistics to assess the degree of asymmetry. Hence the data points with $r \leq 3R_{\text{TDE}}$ for the wider binaries (purple and blue lines in the bottom panels) are not statistically significant. However, these wide binaries contribute a tiny fraction to the total number in the GW regime, which is dominated by the tightest binaries.

is evident that the fraction of merging BBHs is largely dominated in number by the tightest binaries (0.1 au in our study), and hence any global asymmetry will be dominated by the one emerging from those. The three panels of the figure separately show the ratio for the three different masses of the $+$ tertiary considered here. Note that some points for $a_{\text{BH}} = 10$ au are missing from the middle and right panels due to the corresponding areas of the $(-)$ binaries being infinitesimally small, so the ratio cannot be defined.

As indicated by the bottom panel of Figure 5, for tight BBHs with 0.1 au semimajor axes, the ratio $A_{\text{hard},(+),+}/A_{\text{hard},(-),+}$ is very small as BBHs get closer to the SMBH. This is because the outcomes of the scatterings strongly depend on the tidal force exerted on the BBH by the SMBH. For tight binaries with 0.1 au semimajor axes, the orbital velocity of the stellar BH ($\sim 700 \text{ km s}^{-1}$) is very high; therefore, the angular momentum with respect to the SMBH of the inner component and the outer component of the BBH have a larger difference. This increases the efficiency of the tidal hardening in $(-)$ binaries that we discussed in the last section since the outer component of the BBH has lower relative velocity with respect to the SMBH compared to the inner component of the BBH, and therefore it becomes easier to move inward. However, this increases the

efficiency of the tidal softening in $(+)$ binaries. Therefore, a larger number of tight BBHs is expected from the $(-), +$ scatterings.

As already noted (middle panel of Figure 5), for initially widely separated binaries (1 au and 10 au), only a tiny fraction ($<1\%$) of scatterings can produce binaries in the GW regime. Due to the very small event number, the ratio $A_{\text{hard},(+),+}/A_{\text{hard},(-),+}$ for $a_{\text{BH}} = 10$ au and 1 au at $r \leq 3R_{\text{TDE}}$ has large statistical errors which do not make it physically meaningful. This is not problematic for our overall conclusions since the global asymmetry for binaries merging within the Hubble time is dominated by the tight binaries, of which a much larger number enters the GW regime. Whether the ratio $A_{\text{hard},(+),+}/A_{\text{hard},(-),+}$ is larger or smaller than unity for these binaries depends on the preferential location for scattering to happen in the AGN disk, and on the relative mass of the tertiary with respect to that of the binary (cf. bottom panel of Figure 5).

4. Discussion and Conclusions

Almost all dynamical channels for BBH mergers involve spherical symmetry, such that prograde $(+)$ binaries have $(+),+$ or $(+),-$ tertiary encounters at the same rate. Likewise

the rates of $(-), +$ and $(-), -$ encounters should be comparable. Thus, most dynamical BBH merger channels (e.g., in globular clusters or nuclear star clusters) are expected to have a symmetric projected spin distribution χ_{eff} around zero (e.g., Rodriguez et al. 2018). AGN disks are one of the few dynamical channels where asymmetries can arise in encounters (McKernan et al. 2021).

The upper panel of Figure 5 demonstrates that there is an asymmetry in hardening encounters between $(+)$ and $(-)$ binaries and $+$ tertiary encounters as a function of binary semimajor axis. The asymmetry broadly corresponds to: (1) for $r < 5R_{\text{TDE}}$, a preferential hardening of $(-)$ binaries and (2) for $r > 5R_{\text{TDE}}$, a preferential hardening of $(+)$ tight binaries for comparable or slightly smaller $+$ tertiary masses.

If we ascribe the asymmetry in χ_{eff} observed in LIGO–Virgo mergers (Callister et al. 2021; McKernan et al. 2021) to the AGN channel (and hence consider the subset of binaries in the GW regime, bottom panel of Figure 5), then the nature of the asymmetry depends on the efficiency of gas hardening and/or the nature of most dynamical encounters. If a_{BH} is small when a dynamical encounter occurs, then it is more likely to merge within a Hubble time and contribute to the LIGO–Virgo observed rate. Gas hardening of binaries in AGN disks should create a preference for small a_{BH} binaries, though it remains uncertain whether gas hardening will stall prior to the GW hardening regime, and the value of any stalling radius is also uncertain. For binaries at a migration trap (which should occur at $r \gtrsim 5R_{\text{TDE}}$, Bellovary et al. 2016), dynamical hardening encounters are enhanced between $(+)$ binaries and $+$ tertiaries. This implies that preferentially positive χ_{eff} mergers should be produced by the AGN channel. However, if gas hardening is inefficient and stalls at very large a_{BH} , dynamical encounters will produce negligible rates of mergers from the AGN channel.





All of our results apply to a single encounter between a prograde BBH $(+)$ or retrograde BBH $(-)$ with a prograde $+$ tertiary BH. However, we expect multiple encounters in AGN disks to be likely in a short time (e.g., Leigh et al. 2018; Samsing et al. 2020; Secunda et al. 2020; Tagawa et al. 2020b; McKernan et al. 2020). Orbital timescales scale as

$$t_{\text{orb}} \sim 0.5 \text{ yr} (M_{\text{SMBH}}/10^8 M_{\odot}) (R_{\text{disk}}/10^3 r_g)^{3/2}, \quad (3)$$

so multiple encounters could occur at relatively small separations and relative velocities as modeled above. A more complete parameter space study with Monte Carlo sequential multiple encounters will be carried out in future work.

We thank Carl Rodriguez for early discussions of some of the ideas in this paper. Y.W. and R.P. gratefully acknowledge support by NSF award AST-2006839. B.M. & K.E.S.F. are supported by NSF AST-1831415 and Simons Foundation Grant 533845. N.W.C.L. gratefully acknowledges the generous support of a Fondecyt Iniciación grant 11180005, and the financial support from Millenium Nucleus NCN19-058 (TITANs) and the BASAL Centro de Excelencia en Astrofísica y Tecnologías Afines (CATA) grant PFB-06/2007. M.-M.M.L. is partly supported by NSF grant AST18-15461.

ORCID iDs

Yi-Han Wang  <https://orcid.org/0000-0002-8614-8721>
 Barry McKernan  <https://orcid.org/0000-0002-9726-0508>
 Rosalba Perna  <https://orcid.org/0000-0002-3635-5677>
 Nathan W. C. Leigh  <https://orcid.org/0000-0003-0347-276X>
 Mordecai-Mark Mac Low  <https://orcid.org/0000-0003-0064-4060>

References

- Bartos, I., Kocsis, B., Haiman, Z., & Márka, S. 2017, *ApJ*, **835**, 165
 Baruteau, C., Cuadra, J., & Lin, D. N. C. 2011, *ApJ*, **726**, 28
 Bellovary, J. M., Mac Low, M.-M., McKernan, B., & Ford, K. E. S. 2016, *ApJL*, **819**, L17
 Bogdanović, T., Reynolds, C. S., & Miller, M. C. 2007, *ApJL*, **661**, L147
 Callister, T. A., Haster, C.-J., Ng, K. K. Y., Vitale, S., & Farr, W. M. 2021, *ApJL*, **922**, L5
 Dittmann, A. J., & Miller, M. C. 2020, *MNRAS*, **493**, 3732
 Gröbner, M., Ishibashi, W., Tiwari, S., Haney, M., & Jetzer, P. 2020, *A&A*, **638**, A119
 Hills, J. G. 1988, *Natur*, **331**, 687
 Leigh, N. W. C., Geller, A. M., McKernan, B., et al. 2018, *MNRAS*, **474**, 5672
 Leigh, N. W. C., Mastrobuono-Battisti, A., Perets, H. B., & Böker, T. 2014, *MNRAS*, **441**, 919
 Li, Y.-P., Dempsey, A. M., Li, S., Li, H., & Li, J. 2021, *ApJ*, **911**, 124
 Liu, B., & Lai, D. 2017, *ApJL*, **846**, L11
 McKernan, B., Ford, K. E. S., Bellovary, J., et al. 2018, *ApJ*, **866**, 66
 McKernan, B., Ford, K. E. S., Callister, T., et al. 2021, arXiv:2107.07551
 McKernan, B., Ford, K. E. S., Lyra, W., & Perets, H. B. 2012, *MNRAS*, **425**, 460
 McKernan, B., Ford, K. E. S., & O’Shaughnessy, R. 2020, *MNRAS*, **498**, 4088
 Rodriguez, C. L., Amaro-Seoane, P., Chatterjee, S., & Rasio, F. A. 2018, *PhRvL*, **120**, 151101
 Samsing, J., Bartos, I., D’Orazio, D. J., et al. 2020, arXiv:2010.09765
 Secunda, A., Bellovary, J., Mac Low, M.-M., et al. 2020, *ApJ*, **903**, 133
 Stone, N. C., Metzger, B. D., & Haiman, Z. 2017, *MNRAS*, **464**, 946
 Tagawa, H., Haiman, Z., Bartos, I., & Kocsis, B. 2020a, *ApJ*, **899**, 26
 Tagawa, H., Haiman, Z., & Kocsis, B. 2020b, *ApJ*, **898**, 25
 Theuns, T., Boffin, H. M. J., & Jorissen, A. 1996, *MNRAS*, **280**, 1264
 Tiede, C., Zrake, J., MacFadyen, A., & Haiman, Z. 2020, *ApJ*, **900**, 43
 Wang, Y.-H., Leigh, N. W. C., Liu, B., & Perna, R. 2021, *MNRAS*, **505**, 1053
 Yang, Y., Bartos, I., Gayathri, V., et al. 2019, *PhRvL*, **123**, 181101